Universiti Malaysia Terengganu Journal of Undergraduate Research
Volume 4 Number 2, April 2022: 23-36
eISSN: 2637-1138

PASSIVE CONTROL OF VORTEX-INDUCED MOTIONS ON DEEP-DRAFT SEMISUBMERSIBLE PLATFORMS

SITI MASALIZA ANUAR AND MOHD ASAMUDIN A RAHMAN*

Faculty of Ocean Engineering Technology and Informatics, Universiti Malaysia Terengganu, 21030 Kuala Nerus, Terengganu, Malaysia

**Corresponding author: mohdasamudin@umt.edu.my*
https://doi.org/10.46754/umtjur.v4i2.272

Abstract: The deep-draft semisubmersible (DDSS) platform is well known due to its favourable vertical motion routine. However, DDSS platforms face a serious challenge in vortex-induced motion (VIM) due to the changing forces of the column. A computational fluid dynamic (CFD) simulation using AcuSolve is conducted to investigate the effect of a twisted-square column with different twisted angles, 0°, 22.5°, 45.0°, 67.5° and 90.0°, on the VIM responses and performance at current incidence angles of 0° and 45°.Platform models at a scale of 1:70 are studied to determine that the alteration of vortex shedding due the separation line at the twisted column expressively influences the mean and fluctuation of hydrodynamic forces and motion. In particular interest is the drag and lift coefficients, surge, sway amplitudes, as well as the yaw motion of the DDSS platform. The simulation was conducted at a velocity of 0.16 m/s.

Keywords: CFD, VIM, DDSS, Passive control, Twisted-square column.

Introduction

The development of oil and gas in a deep-water field using deep-draft Semisubmersible (DDSS) platforms is increasing in terms of drilling, storage, offloading and production operations. Offshore platforms, also known as oil platforms, are gigantic structures placed in deeper water offshore and are equipped with various types of facilities to drill wells and extract oil and gas. There are many kinds of oil platforms that either float or are fixed on the ocean floor. They include floating production storage and offloading (FPSO) systems, compliant towers, jackup rigs, tension leg platforms, spar platforms and semi-submersible platforms. Semi-submersible platforms, such as in Figure 1, can be moved from one place to another, and they have a hull, made up of columns and pontoons that provide adequate buoyancy to cause the structure to float. It is a self-stabilised structure with advanced motion behaviour and is resistant to waves, wind and current from any direction (Narendran *et al.,* 2018).

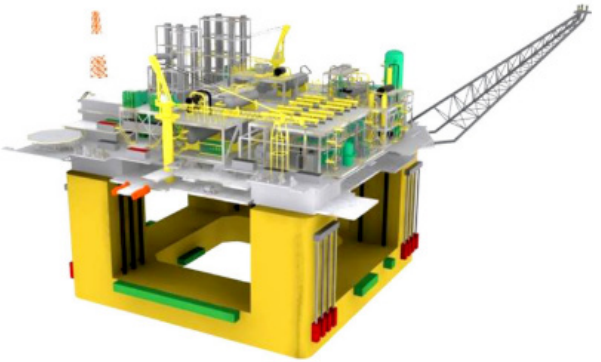

Figure 1: An illustration of a semi-submersible platform with four square columns (Gonçalves *et al.,* 2013)

Numerous studies have been carried out on circular cylinders using active and passive control methods. For the active control technique, external energy is needed to change the vortex wake system and the boundary layer separation, such as suction (Chen *et al.,* 2014; 2015), oscillating foils (Bao & Tao, 2013), synthetic jets (Wang *et al.,* 2016) and distributed forcing (Kim *et al.,* 2005). Passive controls for suppression include helical (Quen *et al.,* 2014), passive, surface roughness (Zhou *et al.,* 2015) and splitter plate (Assi & Bearman, 2015; Law & Jaiman, 2017). What is common in these studies is that they aim to alter the exterior shape of the bluff body to modify the separation point and to interrupt the coherent vortex shedding process (Wu *et al.,* 2018). A twisted square column in DDSS is one of the passive control techniques and is shown in Figure 2.

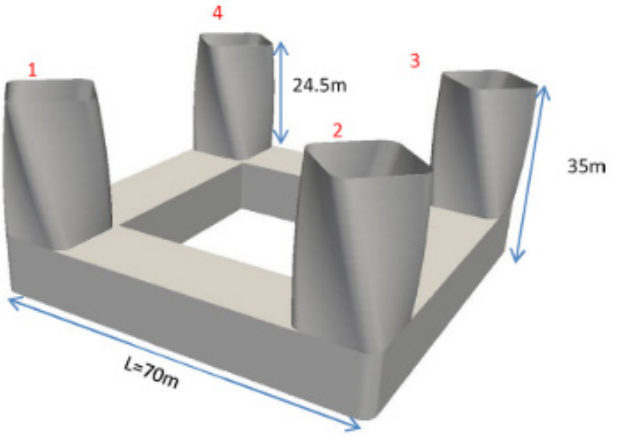

Figure 2: Twisted column in deep-draft semisubmersible platforms (Wu *et al.,* 2018)

Floating offshore platforms shift laterally with a base period of an oscillating force, which is called vortex-induced motion (VIM), which is in contrast to vortex-induced vibration (VIV) in long structures such as a riser (Liu *et al.,* 2017). VIM is a motion that is induced by vortex shedding and occurs on huge offshore floating structures. VIM is described mainly by two degrees of freedom (DOF) in the free surface, which are the in-line (surge) and transverse (sway) directions (Goncalves *et al.,* 2012).

The effects of the sea current environment on the dynamic behaviour of floating structures have become a crucial design issue (Liu *et al.,* 2015). With the need for DDSS, the challenges of VIM have become a major concern in the last two decades. This is due to the impact VIMs can have on structural stability and fatigue damage of risers and mooring lines, which can lead to long operational downtimes for offshore platforms. When a bluff body is exposed to a stream of fluid, changing vortices can shed downstream from one side to other of the structure, which will generate an oscillatory hydrodynamic force.

Materials and Methods

Design Phase

The twisted-square column of DDSS model is created using CAD software RHINO 6. The solid structure of the platform was created with its own dimension. The models were created in a 1:70 scale and the domain for the simulation was created and combined together with the platform to form a solid structure as shown in Figure 3.

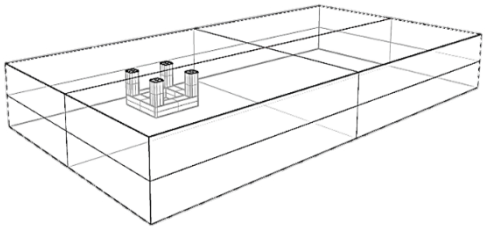

Figure 3: Fluid domain and platform structure

The dimensions of the twisted-square column and the domain for the five case studies are the same. Tables 2 and 3 show the dimension of the twisted-square column of DDSS and the dimension of the domain, respectively.

Table 2: Dimension of the untwisted and twisted-square column of the DDSS

No	Platform Component	Full-Scale Dimension (M)	1:70 Scale (M)
1	Pontoon Length	70.0	1.00
2	Pontoon Height	10.5	0.15
3	Pontoon Width	14.0	0.20
4	Column Height	24.5	0.35
5	Column Width	14.0	0.20
6	Pontoon and Column Radius	14/6	(14/6)/70

Table 3: Dimension of the domain

No	Domain	Scale (M)
1	Length	9.5
2	Width	5.0
3	Height	1.0

Figure 4 shows the twisted-square columns with different twisted angles of the DDSS, which are 0°, 22.5°, 45° ,67.5° and 90°.

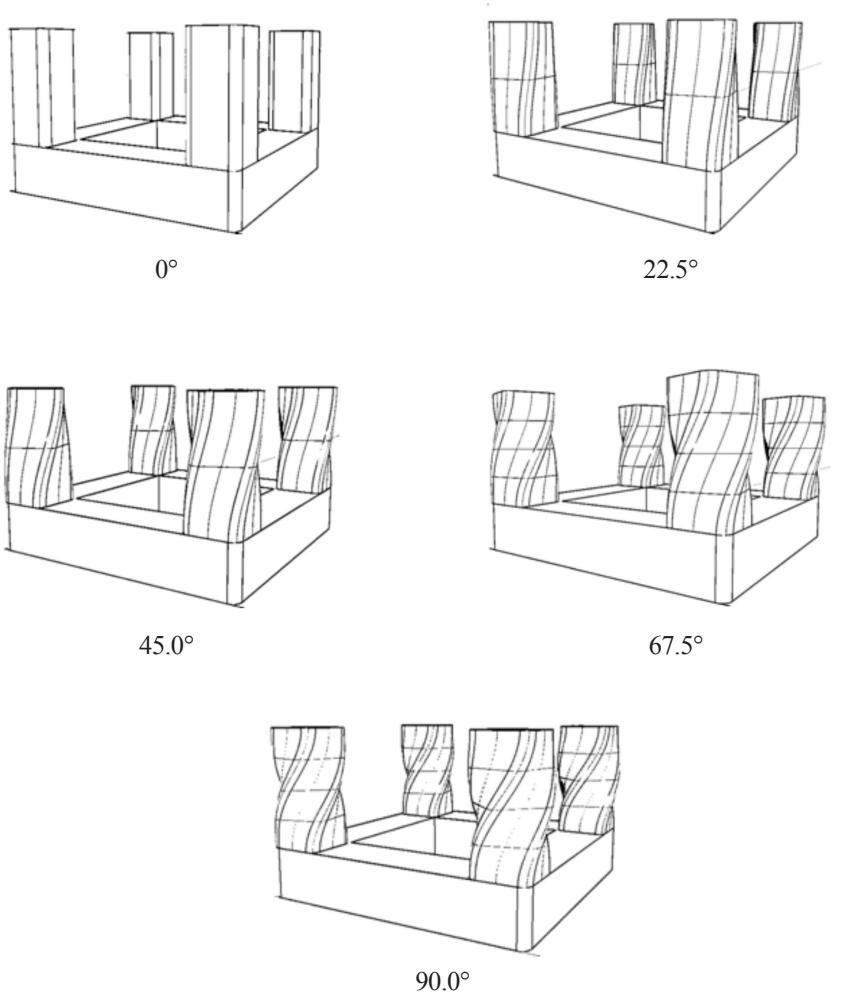

Figure 4: The twisted-square columns of the DDSS

Boundary Condition

All the intricacies in fluid dynamics are governed by the same standard conservation equations. What makes the solution of each problem exclusive is the set of boundary conditions. Hence, the boundary conditions have boundless impacts on the accuracy of the simulation. The boundary conditions of the fluid domain act as the likely conditions in the open sea. In the domain design, there are four boundary conditions, which are the inlet, outlet, symmetry, and wall. The setting of the boundary conditions is shown in Figure 5.

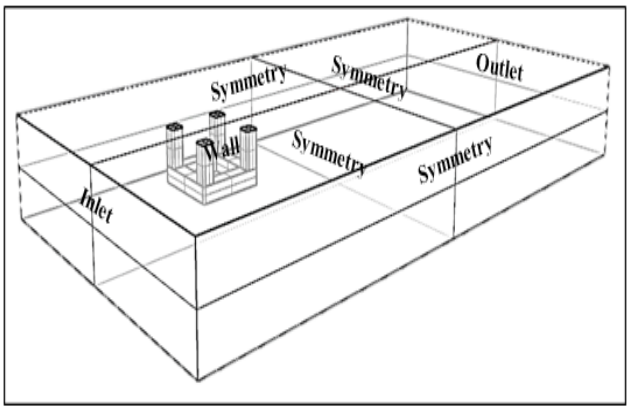

Figure 5: The domain and the structure of the deep-draft semisubmersible with the boundary condition

Simulation Condition

For each case study, the same value of the Reynolds number (Re), which is 23535, was used. Re is in the subcritical regime and can be determined using Equation (1). Re is a dimensionless number used in fluid mechanics to show whether the fluid flow past a body or in a duct is steady or turbulent.

The velocity was set at 0.16 m/s for every case. The density and viscosity were set at 1000 kg/m^3 and 0.0071 kg/m sec. Next, there were two incidence angles, which were 0° and 45°. The incidence angle is a position of the platform in the domain.

Re is determined by using the formula below:

$$Re = \frac{\rho.V.L}{\mu} \quad (1)$$

Where ρ is density, V is velocity, L is length, which is 1m, and μ is the dynamic viscosity.

Mesh Independent Study

The main purpose of the mesh independent study is to find the optimum mesh until the result is approximate to the reference paper. The optimum mesh significantly proved that the simulation is precise. The simple structure, which is a square cylinder, is created and used for this simulation. All the settings are the same as the case studies. Figure 6 shows the design and the dimension of square cylinder with the boundary condition. Figure 7 shows the differences of the mesh generation based on the smallest and highest number of elements, which are 8,000 and 71,000, respectively. The parameters for the mesh independent study are shown in Table 4.

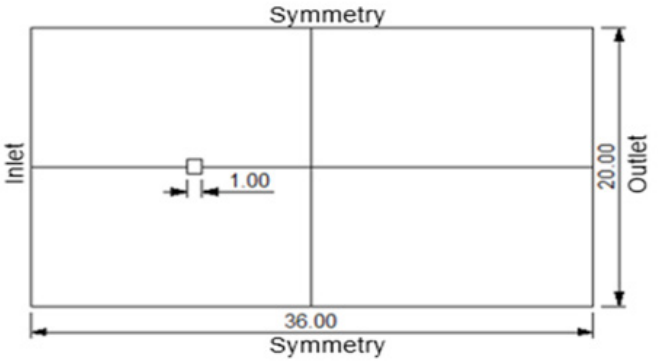

Figure 6: The design and dimension of the square cylinder with the boundary condition

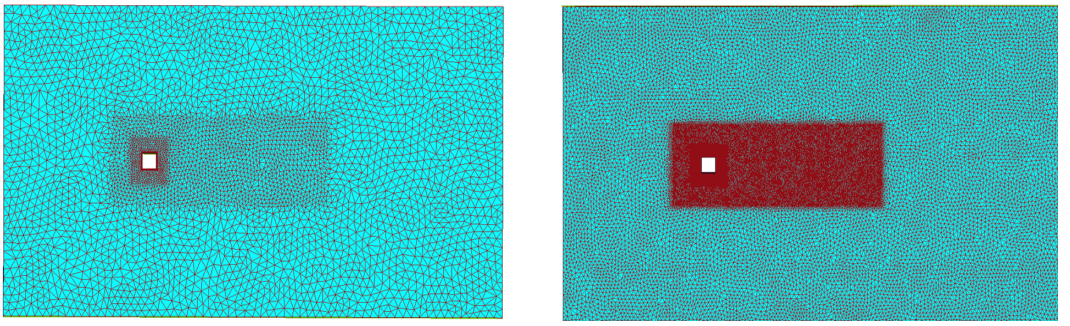

(a) (b)

Figure 7: The mesh generation of the different number of elements of (a) 8,000 and (b)71,000

Table 4: Parameters for the mesh independent study

No	Parameter	Value
1	Reynolds number	100
2	Velocity	1 m/s
3	Viscosity	0.01 kg/m.sec
4	Density	1 kg/m^3

The results showed that the 71,000 number of elements had the lowest value of drag coefficient (Cd), lift coefficient (Cl) and Strouhal number (St). Table 5 shows the mean Cd, Cl rms and St of this study compared with a previous study by Felipse *et al.* (2018). It shows that the highest number of elements, which is 71,000, has the lower percentage error and has a value that is approximate to the reference paper. Figure 8 shows the graph of the Cd, Cl and St compared with previous paper by *Felipe et al.* (2018).

(a)

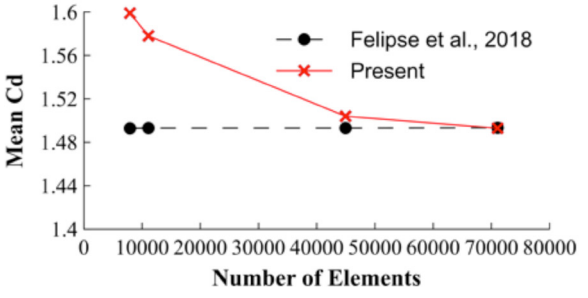

(b)

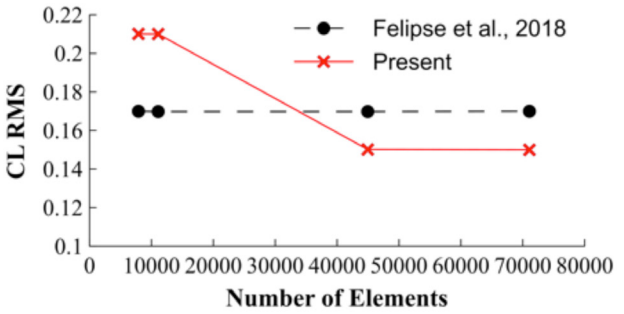

(c)

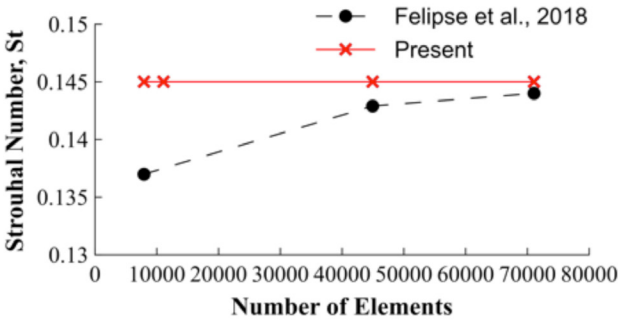

Figure 8: The patterns of Cd, Cl and St of the present results compared with the reference paper

Table 5: The mean Cd, Cl rms and Strouhal number

Number of Element	Mean Cd	Error (%)	Cl, rms	Error (%)	Strouhal number	Error (%)
Felipe *et al.* (2018)	1.50	-	0.17	-	0.145	-
8 000	1.60	6.0	0.21	20.0	0.137	-5.0
11 000	1.58	5.3	0.21	20.0	0.137	-5.0
45 000	1.51	0.6	0.15	-12.0	0.143	-1.0
71 000	1.50	0	0.15	-12.0	0.144	-0.6

Results and Discussion

Comparison of motion at different twisted angles with different incidence angles

Table 6 shows the mean surge amplitude, mean sway amplitude and mean yaw motion that is calculated using the selected formula. The amplitude of the VIM motion is mathematically described by the normalised nominal amplitude, which is a dimensionless number based on the statistically determined standard deviation of y(t) over a sufficiently high number of VIM cycles and the appearances dimension of the platform column, D.

Table 6: Mean Surge, Sway and Yaw

	Mean Surge (m)		**Mean sway (m)**		**Mean Yaw (rad)**	
Twisted-square column (◦)	**Incidence angle (◦)**					
	0	**45**	**0**	**45**	**0**	**45**
0	0.005	0.004	0.012	0.012	0.126	0.072
22.5	0.016	0.003	0.011	0.011	0.173	0.044
45.0	0.009	0.004	0.022	0.012	0.216	0.021
67.5	0.007	0.002	0.022	0.007	0.226	0.021
90.0	0.007	0.002	0.007	0.007	0.108	0.014

The highest value of surge amplitude for incidence angle 0° occurs at the twisted angle of 22.5°, and the value decreases as the twisted angle increases to 90°. For incidence angle 45°, twisted angle 0° and 45° have the highest value of surge amplitude and it decreases as the twisted angle increases to 90°. The 45° incidence angle has a lower surge amplitude value compared with the 0° incidence angle.

The highest value of sway amplitude for incidence angle 0° occurs at twisted angle 45° and the value slowly goes down as the twisted angle increases to 90°. For incidence angle 45°, the 0° and 45° twisted angles have the highest value and it decreases as the twisted angle increases to 90°. The incidence angles *0° and 45°* share the same lowest value of sway amplitude at twisted angle 90°.

The highest value of yaw motion for incidence angle 0° occurs at twisted angle 67.5° and the value decreases as the twisted angle approaches 90°. For incidence angle 45°, the highest value of yaw motion is at twisted angle 0° and the value decreases as the angle approaches 90°. The values of yaw motion for incidence angle 45° are lower than the values of yam motion for incidence angle 0°.

(a)

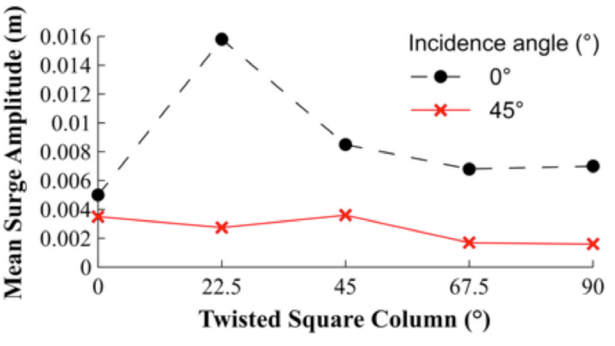

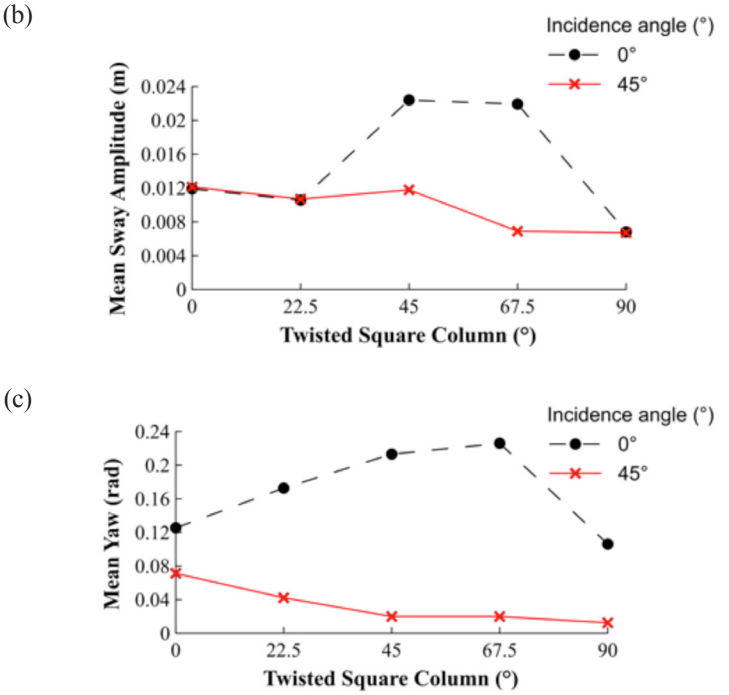

Figure 9: Comparison of a) mean surge amplitude b) mean sway amplitude c) mean yaw at different twisted angles with different incidence angles.

Comparison of forces between different twisted angles with different incidence angles

Two forces were calculated based on the cases, which are drag force, F_d, and lift force, F_L. Drag force is the direction that is opposite to the relative flow velocity, while lift force is in the direction that is perpendicular to the relative flow. From the forces, the drag coefficient, Cd, and lift coefficient, Cl, is calculated using the selected formula. The Strouhal number is the oscillating flow mechanism that is the frequency from the lift coefficient. Figure 10 shows the mean Cd, Cl, amplitude and Strouhal number for every case. For incidence angle 0°, the highest value of Cd occurred at twisted angle 45° and decreases as the twisted angle approaches 90°. For incidence angle 45°, the Cd value decreases from twisted angles 0° to 675°, and peaks slowly at twisted angle 90°. The Cd values at incidence angle 45° were lower than the values at incidence angle 0°.

When the velocity increases, the pressure decreases and it creates Cl. For incidence angle 0°, the higher Cl value occurs at twisted angle 67.5° and the value decreases at twisted angle 45° and slowly increases at twisted angle 90°. For incidence angle 45°, the highest Cl value occurs at twisted angle 0° and it decreases as the angle approaches 90°. The Cl values at incidence angle 0° were higher the the values at incidence angle 45° incidence angle. Higher frequencies of vortex shedding make the Strouhal number, St, higher. For incidence angle 0°, the value of St is the highest at twisted angle *0° and* stays steady from twisted angles 22.5° to 90°. For incidence angle 45°, the highest value of St occurs at twisted angle 0° and the value decreases as the twisted angle approaches 67.5°, but increases slightly at twisted angle 90°. The St values for incidence angle 45° were higher at first, but goes than the values for incidence angle *0° incidence,* which shows a higher value at first and the values remain the same at twisted angles 22.5° to 90°.

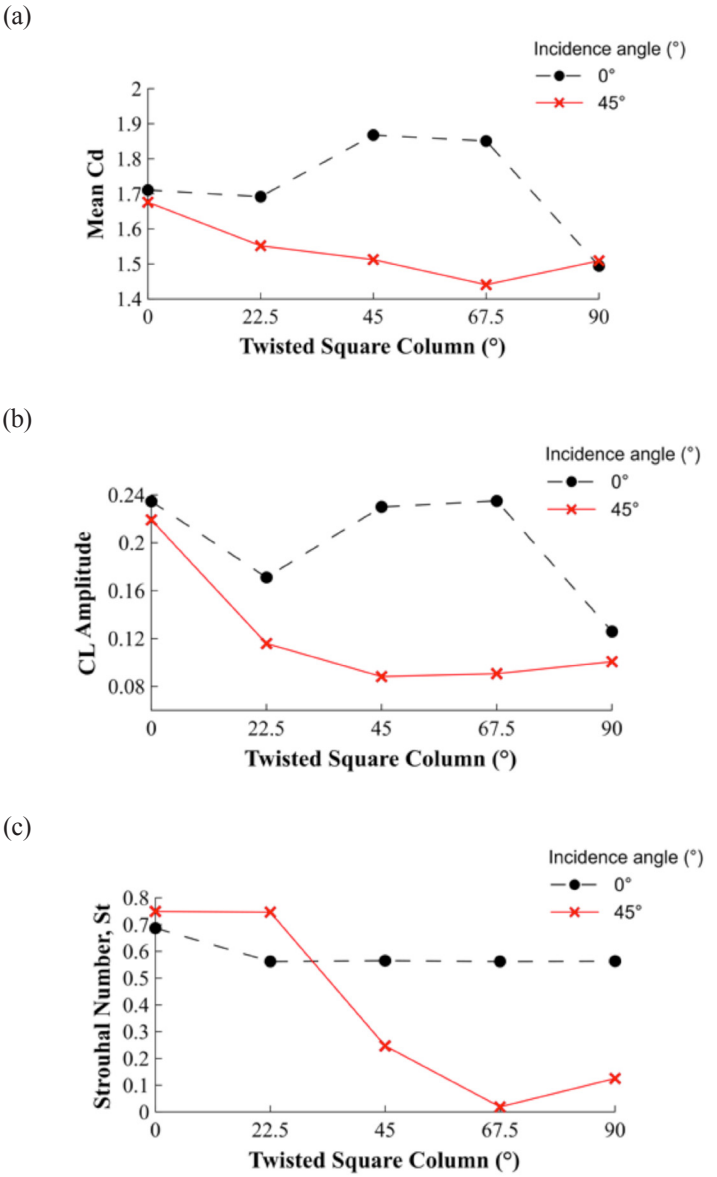

Figure 10: Comparison of a) mean Cd b) Cl amplitude c) Strouhal mumber at different twisted angles with different incidence angles

Visualisation of the velocity contour

The visualisation is conducted to observe the velocity contour acting on the boundary surface. The visualisation is taken at time 30 seconds. Figure 11 below shows the velocity contours for every cases study. We can see that for incidence angle 0°, the flow of water through the platform shows a higher velocity due to the flow separation point acting on the surface, which made a bigger impact and affected the vortex behind the column. For incidence angle 45°, the velocity flow acting on the platform is smaller as the separation point at the curve disperses and disrupts the vortex shedding at the back of the column and it reduces the VIM responses.

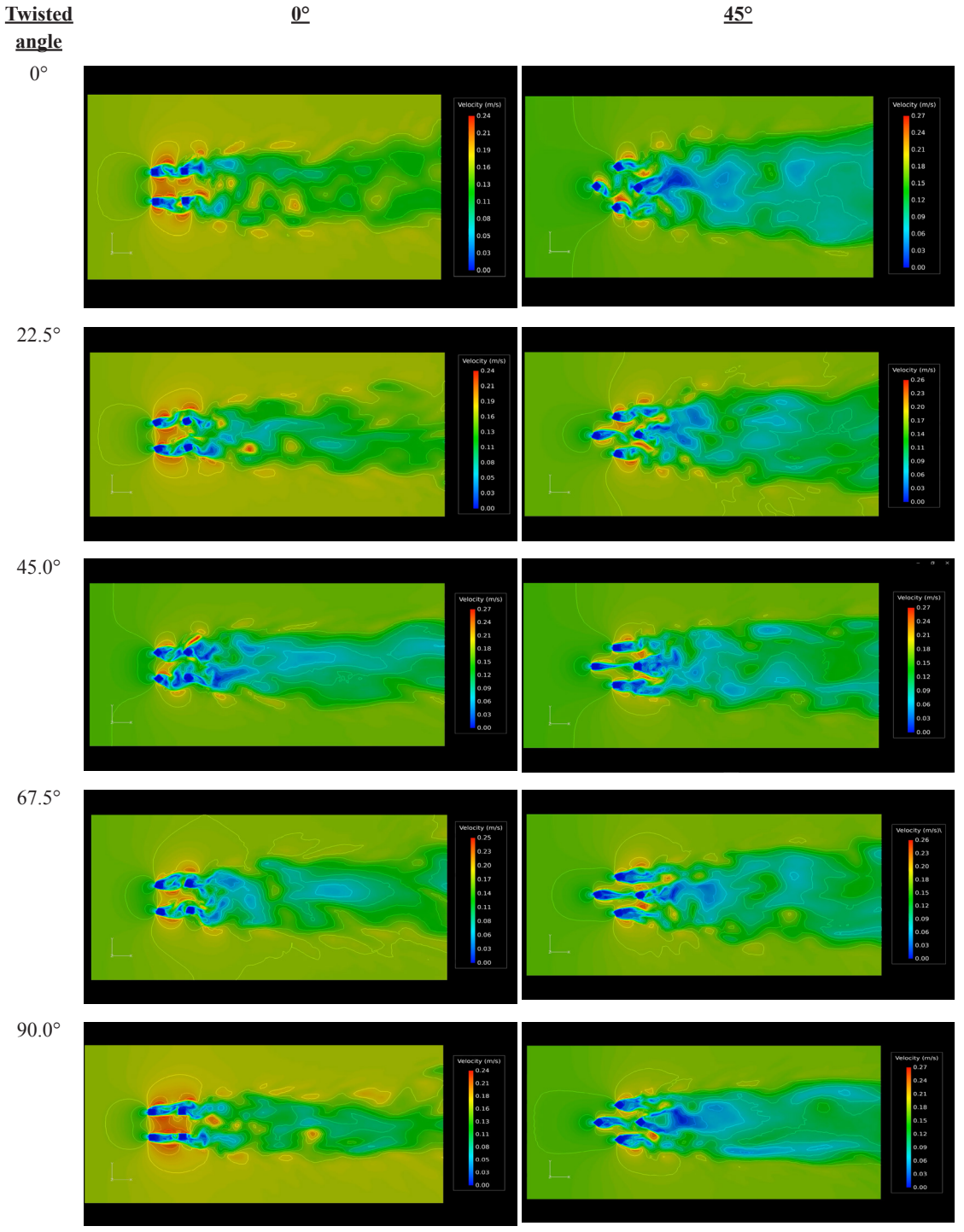

Figure 11: Velociy contours

Conclusion

To control the VIM responses of DDSS platforms in uniform sea currents, different twisted angles with the different incidence angles were studied via LES-based finite volume simulations. Column amplitudes and hydrodynamic forces and motion were found to reduce substantially by the effects of the twisted surface. The separation lines of the twisted columns distribute irregularly and vary as a function of time, which significantly affects the vortex synchronisation. By analysing the values of the forces and motion, and also by visualizing the velocity contours, the twisted surface of the column can induce a variation of separation points along the column span that results in the disruption of vortex synchronisation and reduces the hydrodynamic forces and motion. These effects of the twisted surface on vortex dynamics are significant to effectively control the VIM responses. Based on the results of the simulation, for the first objective, from all the five designs of the twisted angles, the best design to suppress the VIM motion is the twisted angle of 90° due to the different orientation of the twisted column and lower vortex interaction between the columns. For the semisubmersible with twisted columns, the effects of flow incidence angle from the case studies show that the effective incidence angle that can reduce the VIM responses is 45°. The 45° incidence angle can suppress the hydrodynamic motion due to the separation point that occurs at the curve, which will disperse and disrupt the vortex shedding and reduce the VIM responses. Some possible ways to lower the VIM due to wake generation behind the platform pontoon is to switch the square columns to a twisted column angle of 90° with incidence angle of 45°.

Acknowledgements

The authors would like thank supervisor Assoc. Prof. Mohd Asamudin bin A. Rahman for his guidance in completing this project.

References

Assi, G. R. S., & Bearman, P. W. (2015). Transverse galloping of circular cylinders fitted with solid and slotted splitter plates. *Journal of Fluids and Structures, 54*, 263–280. https://doi.org/10.1016/j.jfluidstructs.2014.11.005

Bao, Y., & Tao, J. (2013). Active control of a cylinder wake flow by using a streamwise oscillating foil. *Physics of Fluids*, *25*(5). https://doi.org/10.1063/1.4802042

Chen, W. L., Li, H., & Hu, H. (2014). An experimental study on a suction flow control method to reduce the unsteadiness of the wind loads acting on a circular cylinder. *Experiments in Fluids, 55*(4). https://doi.org/10.1007/s00348-014-1707-7

Chen, W., Cao, Y., Li, H., & Hu, H. (2015). Numerical investigation of steady suction control of flow around a circular cylinder. *Journal of Fluids and Structures*, *59*, 22–36. https://doi.org/10.1016/j.jfluidstructs.2015.09.002

Gonçalves, R. T., Rosetti, G. F., Fujarra, A. L. C., & Oliveira, A. C. (2012). Experimental study on vortex-induced motions of a semi-submersible platform with four square columns, Part I: Effects of current incidence angle and hull appendages. *Ocean Engineering*, *54*, 150–169. https://doi.org/10.1016/j.oceaneng.2012.06.032

González, F. A., Bustamante, J. A., Cruchaga, M. A., & Celentano, D. J. (2019). Numerical study of flow past oscillatory square cylinders at low Reynolds number. *European Journal of Mechanics*, *B/Fluids*, *75*, 286–299. https://doi.org/10.1016/j.euromechflu2018.1

Kim, J., & Choi, H. (2005). Distributed forcing of flow over a circular cylinder. *Physics of Fluids*, *17*(3). https://doi.org/10.1063/1.1850151

Law, Y. Z., & Jaiman, R. K. (2017). Wake stabilization mechanism of low-drag suppression devices for vortex-induced

vibration. *Journal of Fluids and Structures*, *70*(January), 428–449. https://doi.org/10.1016/j.jfluidstructs.2017.02.005

Liu, M., Xiao, L., & Yang, L. (2015). Experimental investigation of flow characteristics around four square-cylinder arrays at subcritical Reynolds numbers. *International Journal of Naval Architecture and Ocean Engineering*, *7*(5), 906–919. https://doi.org/10.1515/ijnaoe-2015-0063

Liu, M., Xiao, L., Lu, H., & Xiao, X. (2017). Experimental study on vortex-induced motions of a semi-submersible with square columns and pontoons at different draft conditions and current incidences. *International Journal of Naval Architecture and Ocean Engineering*, *9*(3), 326–338. https://doi.org/10.1016/j.ijnaoe.2016.11.003

Narendran, K., Guan, M. Z., Ma, P. F., Choudhary, A., Hussain, A. A., & Jaiman, R. K. (2018). Control of vortex-induced motion in multi-column offshore platform by near-wake jets. *Computers and Fluids*, *167*, 111–128. https://doi.org/10.1016/j.compfluid.2018.02.025

Quen, L. K., Abu, A., Kato, N., Muhamad, P., Sahekhaini, A., & Abdullah, H. (2014). Investigation on the effectiveness of helical strakes in suppressing VIV of flexible riser. *Applied Ocean Research*, *44*, 82–91. https://doi.org/10.1016/j.apor.2013.11.006

Wang, C., Tang, H., Duan, F., & Yu, S. C. M. (2016). Control of wakes and vortex-induced vibrations of a single circular cylinder using synthetic jets. *Journal of Fluids and Structures*, *60*, 160–179. https://doi.org/10.1016/j.jfluidstructs.2015.11.003

Wu, C. H., Jaiman, R. K., Lim, T. B. A., Kang, C. W., & Ma, S. (2018). A new passive control technique for the suppression of vortex-induced motion in deep-draft semisubmersibles. *Applied Ocean Research*, *80*, 79–100. https://doi.org/10.1016/j.apor.2018.08.008

Zhou, B., Wang, X., Gho, W. M., & Tan, S. K. (2015). Force and flow characteristics of a circular cylinder with uniform surface roughness at subcritical Reynolds numbers. *Applied Ocean Research*, *49*, 20–26. https://doi.org/10.1016/j.apor.2014.06.002